A Two-Dimensional Analysis of Laser Heat Addition in a Constant Absorptivity Gas

Gregory A. Molvik,* Dochul Choi,† and Charles L. Merkle‡
The Pennsylvania State University, University Park, Pennsylvania

The two-dimensional equations of motion describing the interaction between a laser beam and a flowing gas are considered. An implicit numerical scheme is used to solve these equations for unchoked flow through a converging-diverging nozzle. Separate grids are used for the fluid dynamics and the radiation equations. The effects of beam focusing and cross-beam intensity profiles are included. The calculations are based upon real gas properties for all quantities except the gas absorptivity, which is taken as a constant. The solutions contain the expected hot central core region with cool gas near the walls. This results in steep temperature gradients in both the streamwise and cross-stream directions. The absorption zone acts as a blockage in the nozzle causing a nonuniform velocity profile at the inlet and an overall decrease in mass flow. The absorption region also forces the streamlines to move away from the axis of symmetry, although this effect is not strong.

Introduction

LASER thermal propulsion promises to deliver higher specific impulse from a rocket nozzle than can be attained with conventional chemical propellants. The laser thruster derives its energy by absorbing an incoming beam of electromagnetic radiation, rather than from the combustion process which is utilized in a conventional system. Because its energy supply is external to the working fluid, the heat added per unit mass in the laser engine is not rigidly limited. Instead, the temperature rise and hence, the specific impluse, depends upon the details of the radiation/gasdynamic interaction. This interaction is highly complex and strongly nonlinear. Improved understanding is required if this potentially attractive concept is to be developed. Experimental studies must certainly be undertaken (Refs. 1 and 2 describe experiments currently under way), but analytical results are also necessary to guide and interpret the experimental studies and to scale laboratory results to full-scale applications.

The general picture of a laser thruster is similar to that depicted in Fig. 1. Both the laser beam and the cool unheated gas enter the nozzle from the upstream end. As the gas flows toward the throat, it is heated by absorption of radiant energy, causing it to accelerate. The converging nozzle walls also aid in accelerating the gas. For the space propulsion application, the nozzle remains choked at all times and the flow becomes supersonic downstream of the throat. Although the mixing and recombination phenomena which take place in the supersonic portion of the nozzle are of importance to propulsive performance, they do not affect the absorption process and are considered to be secondary in the present discussion. In an attempt to focus on the radiation/gasdynamic interaction, the present analysis considers the unchoked nozzle where the Mach number remains subsonic throughout. The unchoked nozzle flowfield contains the essential physics of the absorption process and provides considerable insight into this complex interaction. The extension to choked throat conditions is straightforward and requires no additional computational advances.

In a practical laser thruster, the absorption heating will probably be restricted to the region near the centerline of the nozzle, leaving a cool, unheated layer of gas near the wall[3,4] as suggested in Fig. 1. This pattern will produce a highly two-dimensional flowfield. The complexity of the laser/gasdynamic interaction has, however, restricted most of the analyses which have been presented thus far to one-dimensional approximations. Raizer[5] first formulated a low Mach number analysis which was applied briefly in Refs. 6 and 7. The analyses was then generalized by Kemp and coworkers,[8,9] who applied the method extensively to the present problem. Additional applications are given in Ref. 10, and an improved solution procedure is suggested in Ref. 11. Initial attempts at treating some of the two-dimensional effects have included an axisymmetric boundary-layer formulation in Ref. 2 and an enhancement of the original Raizer analysis which allows two-dimensional temperature profiles but retains the one-dimensional fluid dynamic model, in Ref. 12.

The first analysis that considered the complete quasi-one-dimensional equations so that higher Mach numbers could be treated appeared recently.[13] These solutions allowed laser absorption in variable area passages and included the effects of beam convergence. Nevertheless, the one-dimensional formulation cannot handle arbitrary beam shapes and radial intensity variations or the important gradients and mixing phenomena in the direction transverse to the main flow. Some of the important laser propulsion questions which must be answered include an assessment of the fractional power absorbed, estimates of the emission from the heated zone and the magnitude of the radiative heat load on the nozzle walls, a characterization of the stability of the plasma, an estimate of the propagation speed of the heating zone, a quantification of the mixing rates between the hot central core and the cool outer layer of gases, and an assessment of how well the size and peak temperatures of the absorbing volume can be controlled. All these issues are dictated by two-dimensional effects; one-dimensional analyses cannot answer them.

The present paper represents a first step toward extending the one-dimensional formulation of Ref. 13 to this important two-dimensional case. The complete problem is very highly nonlinear and very highly coupled. As a result, its computational solution is extremely difficult. In fact, there has been a serious question as to whether existing algorithms are adequate to treat the problem. Accordingly, one major simplification has been made. The absorptivity of the gas has been taken as a constant. This assumption uncouples the laser beam from the gasdynamics (but does not uncouple the gasdynamics from the laser) and relegates the analysis to a specified heat addition problem. Thus, many of the impor-

Received Feb. 25, 1984; revision received Aug. 30, 1984.

*NASA Computational Fluid Dynamics Trainee.
†Ph.D. Candidate, Mechanical Engineering Department.
‡Professor, Mechanical Engineering Department.

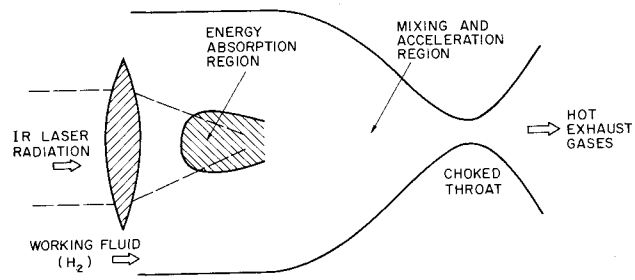

Fig. 1 General characteristics of laser thruster.

tant two-dimensional characteristics itemized above cannot be studied with the present formulation. These calculations are, however, considered a necessary first step toward the eventual resolution of these difficulties, and the results do provide understanding of some aspects of this complicated problem. Appropriate analyses of the laser problem are discussed at length in Ref. 14, and the present approach corresponds to the phase I analysis suggested there.

In addition to the constant absorptivity assumption, the present analysis also contains several more minor simplifications. The guiding principles used in making these additional simplifications have been that they do not further compromise the physics and that they do not omit any additional computational difficulties. In particular, an effort was made to ensure that the only computational difficulty which remains undemonstrated is the effect of variable absorptivity. The precise problem formulation chosen and the computed results are described in the following sections.

Problem Formulation

The formulation studied includes the complete two-dimensional equations of motion for the fluid dynamics and the radiation. Both the effects of viscosity and thermal conductivity are included, along with a capability for arbitrary beam geometries. The working fluid is assumed to be pure hydrogen and appropriate real gas properties are used for all quantities except the gas absorptivity. The results of a constant absorptivity calculation cannot be quantitatively accurate, but they do contain the proper global flowfield characteristics and are useful for obtaining improved physical understanding. As indicated above, even with the constant absorptivity assumption, the flowfield with its dominant heat addition remains an extremely difficult computational problem. The present calculations thus serve two purposes: First, the results provide understanding of some aspects of this complicated problem; and second, they demonstrate the feasibility of computing flowfields that contain the same kinds of strong thermodynamic variations that are representative of the physical problem.

One particular difficulty which is encountered in computing the laser interaction problem is the difficulty of specifying appropriate initial conditions for the calculation. In the presence of realistic gas absorptivities, the present numerical formulation, like the corresponding experimental realization, admits multiple solutions. For example, if a focused laser beam is propagated through a cold gas, it will be transmitted almost without attenuation, whereas if the gas is preheated to breakdown (say, by a spark), the incoming laser energy can maintain breakdown indefinitely and will be strongly absorbed. This effect is well established experimentally. Similarly, with the numerical solutions, a high-temperature initial condition at the appropriate spatial location is needed to initiate the absorption phenomenon. The location and strength of this initial "spark" which leads to stable absorption is difficult to determine. The specification of constant absorptivity eliminates these multiple solutions and the subsequent sensitivity to initial conditions. An important aspect of these constant absorptivity solutions is for use in developing appropriate initial conditions for variable absorptivity calculations which will be atempted at a later date. Meanwhile, the details of the constant absorptivity solutions can begin to answer some of the questions regarding the two-dimensional absorption phenomena.

The additional simplifications that were made in the present calculations are that 1) a slip condition was imposed at the nozzle walls; 2) the formulation is for a planar, not an axisymmetric nozzle; and 3) the effect of radiant emission from the heated gas was ignored. The inviscid boundary condition avoids the development of a boundary layer and the resultant requirement for a highly refined grid near the walls. This allows concentration to be focused on the central heating zone.

The use of a two-dimensional (planar) form of the equations of motion was chosen even though they are slightly easier to treat than the axisymmetric equations. The axisymmetric equations are, however, routinely treated in numerous publications, and the judgment here was to solve the absorption problem without this added detail.

The effect of radiant emission from the heated gas (and the likely reabsorption of this radiation by the surrounding cooler gases) must certainly be incorporated in a complete analysis, but because the constant absorptivity renders the present calculations quantitatively inaccurate, and because this heat loss from the hot regions is a stabilizing effect which makes the calculations easier, it was ignored.

The use of real gas properties was considered a critical part of the feasibility study and their effects were included. The equations for flow in a variable area duct were also solved. Variable area capability is again considered a critical aspect of the complete calculation because calculations in a constant area duct omit many important aspects of the problem of interest and would not allow the propulsion problem to be studied.

Fluid Dynamic Equations

The flow through the converging-diverging nozzle is described by the Navier-Stokes equations. The presence of the laser beam adds a source term to the energy equation, but otherwise the equations are unchanged from their standard form. The primary reasons for including transport properties are that heat conduction can be important in the propagation of the energy absorption region, while viscous effects can be significant in the mixing between the hot central core and the cool outer gases. Since heat conduction is a maximum in the streamwise direction while viscous diffusion occurs most rapidly in the cross-stream direction, parabolized or partially parabolized approximations cannot be used. The complete Navier-Stokes must be treated.

For computational convenience, the fluid dynamic equations are expressed in a body-fitted coordinate system while the radiation equation is expressed in a coordinate system following the rays. In the body-fitted system, the Navier-Stokes equations are

$$\frac{\partial Q}{\partial t}+\frac{\partial E}{\partial \xi}+\frac{\partial F}{\partial \eta}=H+\frac{\partial R}{\partial \xi}+\frac{\partial S}{\partial \eta} \tag{1}$$

where

$$Q=J^{-1}(\rho,\rho u,\rho v,e)^T \tag{2}$$

and

$$E=J^{-1}\begin{bmatrix}\rho U\\ \rho uU+\xi_x p\\ \rho vU+\xi_y p\\ (e+p)U\end{bmatrix} \qquad F=J^{-1}\begin{bmatrix}\rho V\\ \rho uV+\eta_x p\\ \rho vV+\eta_y p\\ (e+p)V\end{bmatrix} \tag{3}$$

Here J is the Jacobian of the transformation which is related to the metrics ξ_x, ξ_y, η_x, and η_y as

$$J=\xi_x\eta_y-\eta_x\xi_y \tag{4}$$

and standard notation has been used for the pressure, density, and velocity components. The total energy e is defined in terms of these quantities and the internal energy ϵ,

$$e=\rho[\epsilon+(u^2+v^2)/2] \tag{5}$$

The contravariant velocities U and V are given by

$$U=\xi_x u+\xi_y v, \qquad V=\eta_x u+\eta_y v \tag{6}$$

The terms on the right-hand side of Eq. (1) include the source term H and the viscous terms R and S. The source contains only the heat addition due to laser absorption,

$$H=J^{-1}(0,0,0,kI)^T \tag{7}$$

where k is the gas absorptivity and I is the laser beam intensity. The viscous terms are the same as those given in Ref. 15. The transformed vectors R and S are given in terms of the Cartesian vectors $\bar{R}$ and $\bar{S}$ as:

$$R=J^{-1}(\xi_x\bar{R}+\xi_y\bar{S}), \qquad S=J^{-1}(\eta_x\bar{R}+\eta_y\bar{S}) \tag{8}$$

where

$$\bar{R}=(0,\tau_{xx},\tau_{xy},R_4)^T, \qquad \bar{S}=(0,\tau_{xy},\tau_{yy},S_4)^T \tag{9}$$

The shear stresses are then defined as

$$\tau_{xx}=4/3\mu u_x-2/3\mu v_y, \qquad \tau_{xy}=\mu(u_y+v_x)$$
$$\tau_{yy}=-2/3\mu u_x+4/3\mu v_y \tag{10}$$

and the transport terms in the energy equation are

$$R_4=u\tau_{xx}+v\tau_{xy}+\kappa T_x, \qquad S_4=u\tau_{xy}+v\tau_{yy}+\kappa T_y \tag{11}$$

Here, the second viscosity coefficient λ has been taken as $\lambda=-2/3\ \mu$, and κ is the thermal conductivity.

The system is closed by specifying an appropriate equation of state and by defining the property variations. Pure hydrogen has been selected as the working fluid of interest for the present calculations, and its equation of state is taken as the perfect gas relation,

$$p=\rho RT/M \tag{12}$$

Because of the high temperatures, the molecular weight M is a variable, and its variation, as well as that of the internal energy, is obtained from thermodynamic relations for equilibrium hydrogen.[9] Conceptually these functions are given as

$$\epsilon=\epsilon(T,p), \qquad M=M(T,p) \tag{13}$$

Similarly, the viscosity and thermal conductivity are also given as functions of the thermodynamic state,[9]

$$\lambda=\lambda(T,p), \qquad \mu=\mu(T,p) \tag{14}$$

The equations describing the variation of radiation intensity are given in the following subsection.

Radiation Equations

The equations governing the local intensity of the laser beam at any point in the nozzle are obtained from geometric optics. The incoming beam is split into a number of separate rays, each propagating in a straight line, as suggested in Fig. 2. For the present calculations, the width of each ray and, hence, its intensity, was assumed to be constant in the absence of absorption. This model simulates the increased intensity of the total beam as it nears the focal point by the mutual overlapping of the rays. In the presence of absorption, the local intensity of each ray is given by

$$dI_m/ds=-kI_m \tag{15}$$

where s represents the distance along the path of the ray, and the subscript m refers to the mth ray. Although this approach gives the correct beam intensity in the limit of an infinite number of beams, it should be noted that more rapid convergence to the limit could be obtained by allowing each of the rays to converge as they neared the focal point. Although this approach is more accurate, it is more complicated geometrically and so was not used in these constant absorptivity calculations. [The convergence of the beams would add an additional 1/s term to the right-hand side of Eq. (15) as was noted by a reviewer.]

The initial intensity of each ray must be specified. For the present calculations, beams with triangular intensity profiles rising linearly from zero at the beam edge to a maximum on the centerline, as illustrated in Fig. 3, were considered. Other intensity distributions (for example, Gaussian) can easily be incorporated. The only requirement is that the initial intensity of each ray be chosen properly.

The focal point of the beam can likewise be chosen arbitrarily by selecting the point or region where the individual rays intersect the symmetry line. Downstream of the focus, a "reflected" ray corresponding to radiation originating in the opposite half of the beam enters the computational domain.

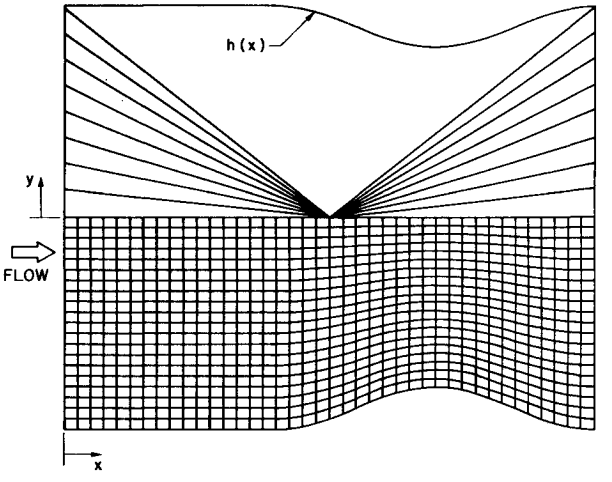

Fig. 2 Nozzle shape and beam geometry. Lower half of figure shows numerical grid for fluid dynamics solution: upper half shows rays used for beam calculation (note only every other ray is shown).

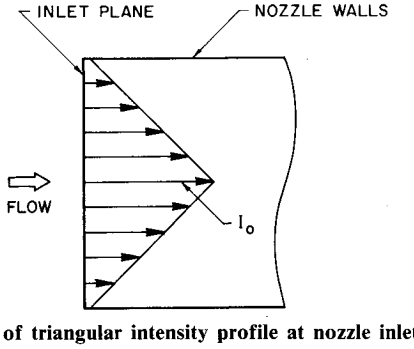

Fig. 3 Detail of triangular intensity profile at nozzle inlet plane.

For the present calculations, the incoming beam was split into 20 rays of equal area. (Note that other choices, including equal power in each ray or other unequal area divisions, could also be made.)

Solution of Fluid Dynamic Equations

Although the fluid dynamic equations are formulated in the complete unsteady sense, only steady solutions are considered in the present paper. These solutions are obtained by applying an implicit, time-dependent scheme[16,17] to Eq. (1). The algorithm chosen is a Euler implicit scheme. In delta notation, it becomes,

$$[I+\Delta t(\delta_\xi A+\delta_\eta B)]\Delta Q=-\Delta t[\delta_\xi(E-R)+\delta_\eta(F-S)-H]^n \tag{16}$$

where δ_ξ and δ_η represent central differences, and A and B are the Jacobians of the flux vectors E and F.

These equations were solved at each time-step by applying a vectorized form of the Douglas-Gunn approximate factorization[16-18] which is consistent on both the intermediate step and the full step. In solving Eq. (16), the source term is treated explicitly. This simplification is possible because the absorptivity is taken as a constant. When the absorptivity depends upon the thermodynamic state of the flowfield, the source term is strongly coupled to the flow and must be treated implicitly. The scheme presented in Eq. (16) and its approximate factorization can be extended to account for this additional complexity.

An additional point to note in regard to Eq. (16) is that the viscous terms have also been treated explicitly. This renders the algorithm conditionally stable, but diffusivities are small enough (Reynolds numbers are high enough) that the optimum time-step is still set by the convective terms. If no-slip conditions were specified at the wall and the wall boundary layers were resolved, this would no longer be true and the viscous terms would also have to be treated implicitly.

Boundary Conditions

The boundary conditions were enforced using the method of characteristics treatment of Chakravarthy[19] and Rai and Chaussee.[20] (Note the unsteady equations are always hyperbolic in time even though they are elliptic in space in the present application.) Proper treatment at the boundaries is extremely important to convergence. For the upstream and downstream formulation, Eq. (16) was premultiplied by the modal matrix, M_ξ, containing the left eigenvectors of the Jacobian $A=\partial E/\partial Q$. The resulting set of characteristic equations was then premultiplied by a selection operator L that selected only the information corresponding to the outgoing characteristics. When the eigenvalues of A are expressed in the order, U, U, $U+c$, $U-c$ (where c is the speed of sound evaluated for variable properties), the selection operator L_u at the upstream boundary takes the form (for subsonic inflow)

$$L_u=\text{diag}(0,0,0,1) \tag{17}$$

Upon premultiplying Eq. (16) by these two matrices, we obtain symbolically

$$L_uM_\xi[\text{LHS Eq. (16)}]=L_uM_\xi[\text{RHS Eq. (16)}] \tag{18}$$

This expression represents one relation for the four state variables Q at the upstream end. The additional three relations must be obtained from the boundary conditions which are here chosen as

$$p^0=\text{const};\quad h^0=\text{const};\quad \tan^{-1}v/u=0 \tag{19}$$

These boundary conditions are analogous to typical experimental conditions where the gas comes from an upstream plenum. The flow angle boundary condition is acceptable for a nozzle with a straight section at the inlet.

Following Refs. 19 and 20, the boundary conditions, Eq. (19), are expressed in the vector form

$$\Omega(Q)=0 \tag{20}$$

where Ω is a vector that contains the three relations in Eq. (19) in the top three rows and a zero in the last row. The Jacobian of Eq. (20) yields a relation in delta form for the remaining three conditions at the upstream boundary.

$$\frac{\partial\Omega}{\partial Q}\Delta Q=-\Omega^n \tag{21}$$

When Eq. (21) is added to Eq. (18), the result is four equations for the four state variables at the upstream boundary.

The downstream boundary is handled in an analogous fashion. At the downstream end, three characteristics arrive from the interior if the outflow is subsonic. The downstream selection operator L_d then becomes

$$L_d=\text{diag}(1,1,1,0) \tag{22}$$

The single boundary condition imposed at the downstream end was the static pressure,

$$p=\text{const} \tag{23}$$

This boundary condition was also expressed in terms of the change ΔQ by the procedure in Eqs. (20) and (21), again giving four equations for the change in the state variables at the downstream boundary.

Along the nozzle wall, this characteristic form was also used, but here Eq. (16) was premultiplied by the modal matrix M_η, containing the eigenvectors of the Jacobian, $B=\partial F/\partial Q$. The boundary condition specified at the wall was flow tangency. The centerline was handled by imposing a symmetry condition.

Solution of Radiation Equations

The radiation equations were discretized in space along each ray. Grid points for each ray were placed midway between the constant ξ-lines in the fluid dynamic grid (see Fig. 4). The heat absorbed from one ray between the two adjacent constant ξ-lines of the fluid dynamic grid was deter-

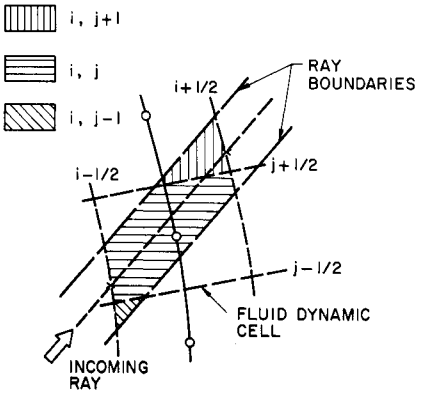

Fig. 4 Detailed definition of radiation grid and its relation to fluid dynamic grid. Crosshatched areas indicate the fluid dynamic cell to which absorbed energy is added. Fluid dynamic grid points are denoted by circles, radiation grid points by crosses.

mined from the local intensity, the path length, and the absorptivity. Finally, the heat added to each fluid dynamic cell was calculated from the percent of the ray which lay in each fluid cell, as illustrated in Fig. 4. This procedure guaranteed conservation of energy and proved efficient to use. Because the absorptivity was constant, the heat addition was uncoupled from the flowfield and could be computed once and for all at the outset of the calculation.

Nozzle and Beam Geometry

The nozzle geometry and the corresponding grid system chosen for the laser absorption analysis are shown in Fig. 2. The nozzle shape was defined by a straight-line section followed by a cosine curve. Mathematically, the nozzle height h is given by the equations

$$h = h_0 \text{ for } 0 \le x \le x_s$$

$$h = h_0 - (1-r)\left\{\frac{h_0}{2}\left[1-\cos\left(2\pi\frac{x-x_s}{x_f-x_s}\right)\right]\right\} \text{ for } x_s \le x \le x_f \tag{24}$$

where r is the area ratio of the nozzle, h_0 is the height of the inlet, and x_s and x_f correspond to the location of the start and end of the converging-diverging section. The area ratio is defined as the ratio of the throat area to the inlet area.

The present calculations are for an area ratio $r=0.8$, with $x_s=100$ mm and $x_f=250$ mm. This corresponds to a total length of 250 mm. The inlet height h_0 was chosen as 100 mm. The throat occurred at $x=175$ mm and its height was 80 mm. A simple algebraic transformation was used to map the nozzle from the physical plane to the computational plane. This transformation is given by

$$\xi = \frac{x}{x_f} \qquad \eta = \frac{h(x)-y}{h(x)} \tag{25}$$

The outline of the focused laser beam is shown in Fig. 2. The laser is focused at $x=119$ mm. As previously mentioned, the incoming laser intensity has been taken as triangular in shape. Calculations have been made for no incoming beam (cold-flow case) and for peak values of $I_0=0.1$, 1.0, and 1.5×10^{10} W/m^2 on the centerline. The width of the laser beam prior to convergence approximately filled the inlet as can be seen from Figs. 2 and 3. In the calculations, the gas absorptivity has been taken as zero in the region $x<25$ mm, thus simulating an "ignition" location. Downstream of this point, the absorptivity was set at $k=23$ m^{-1}. This ensures that approximately 99% of the laser power is absorbed before it reaches the throat.

To document the nature of this heat addition, a contour plot of the absorbed power is shown in Fig. 5. This plot shows that the maximum rate of absorption occurs on the centerline near the upstream end of the heat absorption regions. Lesser amounts of absorption occur toward the edges of the beam where the incoming beam is less intense and toward the focus where the laser energy has been nearly absorbed. This pattern differs from that expected in a variable absorptivity gas where the heat absorption would rise continuously from zero at the upstream end of the absorption region and would attain a maximum toward the middle. The radial falloff in absorbed energy is, however, realistic.

Results and Discussion

A series of computations for the nozzle geometry described above are presented. For these cases, the upstream stagnation pressure was set at 1.04×10^6 N/m^2, the upstream stagnation temperature was 6250 K, and the downstream static pressure was 1×10^6 N/m^2. This stagnation temperature is, of course, unrealistically high for a real application, but its use is justified on several grounds. First, this temperature was chosen to force the upstream boundary conditions to be enforced at a point on the enthalpy-temperature curve where the variation of γ (the ratio of specific heats) was near one of its maximums so we could be sure the upstream boundary-condition specification was proper for a variable property gas. Specification of stagnation enthalpy is no different in a variable property gas than in the constant specific case, but stagnation pressure is somewhat more difficult when γ varies rapidly. The second reason for choosing this high initial temperature was to pave the way for eventual variable absorptivity calculations. Such a high inlet temperature would be beneficial if physical gas absorptivities were used because it would eliminate the very low absorptivity portion of the curve. Thus, the present calculations could be computed more easily for the variable absorptivity case and would allow a useful comparison between the constant and variable absorptivity cases. Finally, it is noted that the level of temperature is somewhat meaningless in the constant absorptivity case; nevertheless, a more realistic temperature would be around 2000 K, assuming the entering hydrogen had been used for regenerative cooling of the nozzle.[21]

The flowfield for the cold flow case (no laser beam) is shown in Fig. 6. The top half of Fig. 6 shows the constant temperature profiles, while the bottom half shows the constant Mach number contours. In the absence of heat addition, the temperature is nearly constant as might be expected. Only the acceleration through the throat region affects the temperature. The fluid nearest the walls in the throat region where the velocity is a maximum is slightly cooler than elsewhere.

The Mach number profiles for the cold flow case also show expected trends, but the levels are of particular interest for comparison with the laser absorption cases. The Mach number at the inlet ranges between 0.36 at the wall and 0.37

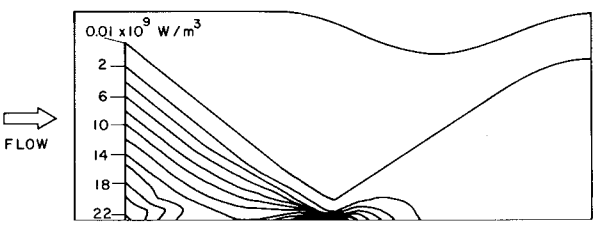

Fig. 5 Contour plot of heat absorbed.

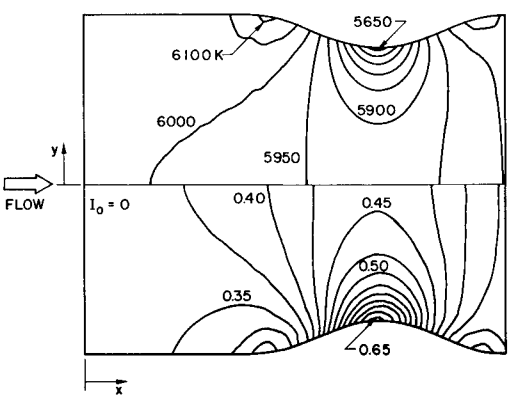

Fig. 6 Constant Mach number contours (lower half), Mach number increment, 0.025; and constant temperature contours (upper half), temperature increments, 50 K; for unchoked nozzle. No laser heat addition.

at the centerline. Thus, without laser heat addition, the flow at the inlet is slightly faster near the centerline of the nozzle than at the wall. This is because the flow near the wall has already begun to anticipate the deceleration where the nozzle convergence begins. At the throat, the Mach number varies from a maximum of 0.66 at the wall to a low of 0.45 at the centerline. This type of Mach number profile is also to be expected. The convex curvature in the throat region accelerates the flow near the walls to velocities considerably higher than are observed on the centerline.

The flowfield for a weak laser beam, $I_0 = 0.1 \times 10^{10}$ W/m^2 at the peak, is shown in Fig. 7. Again, the constant temperature contours are shown in the top half, while the constant Mach number contours are given in the bottom half. In comparison with the laser-off case, the incoming Mach number is lower across the entire nozzle inlet. The heat addition behaves much like a blockage on the axis of the nozzle to cause this effect. Figure 7 shows that the Mach number at the entry is again nearly uniform but that the flow on the centerline is now slightly slower than the wall region—an observation opposite to that noted for the laser-off case.

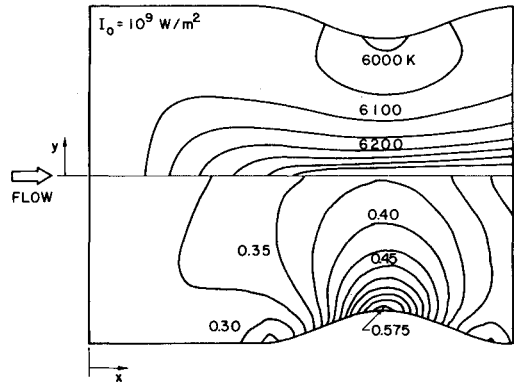

Fig. 7 Constant Mach number contours (lower half), Mach number increment, 0.025; and constant temperature contours (upper half), temperature increment, 50 K; for unchoked nozzle. Triangular laser intensity profile with maximum intensity, $I_0 = 1 \times 10^9$ W/m^2 on centerline.

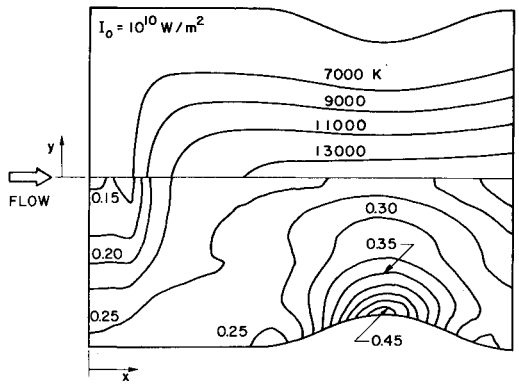

Fig. 8 Constant Mach number contours (lower half), Mach number increment, 0.025; and constant temperature contours (upper half), temperature increment, 2000 K; for unchoked nozzle. Triangular laser intensity profile with maximum intensity, $I_0 = 1 \times 10^{10}$ W/m^2 on centerline.

The temperature profiles in Fig. 7 clearly show the heat addition zone which results in a hot central core region and a cool wall layer. With this relatively low laser energy input, the peak temperature reaches only about 7400 K corresponding to about a 1200 K increase.

The results of the third case are given in Fig. 8 in the same format. The laser intensity used here was 1×10^{10} W/m^2 on the centerline. Here, the peak temperature is nearly 14,500 K, a value which is approaching temperatures characteristic of inverse bremsstrahlung absorption in hydrogen.[1] The Mach number at the inlet plane is considerably skewed. Near the wall it has dropped to 0.25, while at the centerline it is only 0.15. The blockage effect of the heat addition zone is becoming quite large. At the throat the Mach number decreases from a maximum value of 0.47 on the wall to 0.26 on the centerline. Even with this amount of heating, the peak Mach number is decidedly the result of the nozzle convergence, not the heat addition.

The profiles for the final case, $I_0 = 1.5 \times 10^{10}$ W/m^2, corresponding to a peak equilibrium temperature of over 17,000 K, are shown in Fig. 9. Here the effects noted earlier have become more accentuated. At the inlet the Mach number ranges between 0.119 and 0.237. At the throat it reaches a peak value of 0.440 on the wall and is 0.222 on the centerline.

For comparison, the values of the Mach number, temperature, and pressure at the upstream end and at the throat are summarized in Table 1. Values are given for the grid points on the wall and on the centerline. For all cases in the table, the parameters varied monotonically across the channel between the wall and centerline values listed. The mass flow through the nozzle is also included in Table 1.

The cross-stream temperature profiles for the $I_0 = 1 \times 10^{10}$ W/m^2 intensity case are replotted in different fashion in Fig. 10. This figure shows the cross-stream variation of the temperature profile at several axial locations upstream of and at the throat. Recall that the throat occurs at $x = 175$ mm.

All of the calculations presented here are for a 41×21 mesh, and were continued for 400 time-steps. The convergence of the scheme proved to be nearly the same for all cases. A specific example, corresponding to the highest intensity case (1.5×10^{10} W/m^2) is shown in Fig. 11. This figure shows the change $\Delta Q/Q$ in the four components of the vector Q as a function of time-step. The component

Table 1 Tabulated results for pressure, temperature, Mach number, and mass flow

Laser intensity, W/m^2		Mach number		Temperature, K		Pressure, N/m$^2 \times 10^{-6}$		Mass flow, kg/s/m
		Wall	℄	Wall	℄	Wall	℄	
0	Upstream boundary	0.356	0.369	6,020	6,000	1.003	1.000	6.70
	Throat	0.664	0.446	5,630	5,920	0.788	0.952	
0.1×10^{10}	Upstream boundary	0.322	0.310	6,060	6,070	1.010	1.012	6.50
	Throat	0.593	0.375	5,730	7,410	0.828	0.965	
1.0×10^{10}	Upstream boundary	0.252	0.148	6,130	6,210	1.022	1.035	3.70
	Throat	0.466	0.262	5,860	14,340	0.895	0.983	
1.5×10^{10}	Upstream boundary	0.237	0.119	6,145	6,222	1.024	1.038	3.45
	Throat	0.440	0.222	5,898	17,689	0.907	0.987	

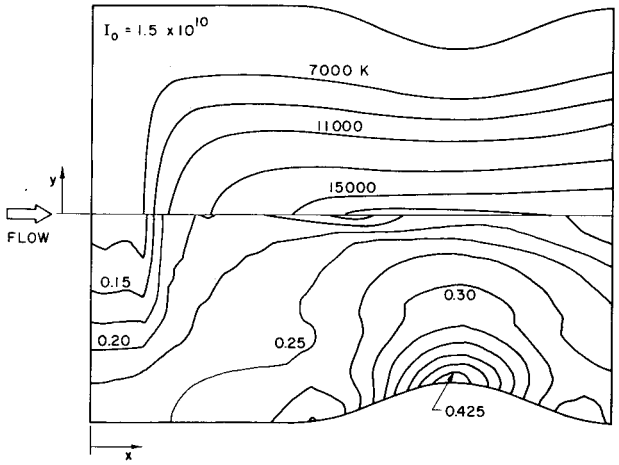

Fig. 9 Constant Mach number contours (lower half), Mach number increment, 0.025; and constant temperature contours (upper half), temperature increment, 2000 K; for unchoked nozzle. Triangular laser intensity profile with maximum intensity, $I_0 = 1.5 \times 10^{10}$ W/m^2 on centerline.

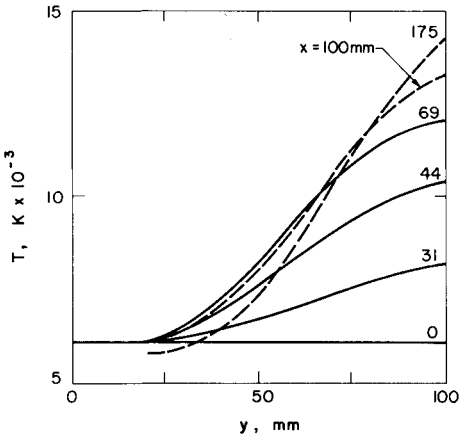

Fig. 10 Cross-stream temperature profiles at various streamwise locations. Maximum laser intensity, $I_0 = 1 \times 10^{10}$ W/m^2. (Note: throat is at $x = 175$ mm.)

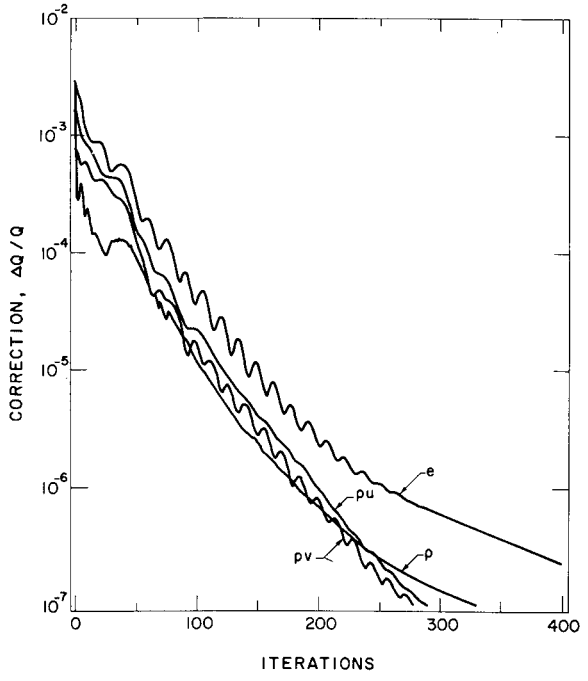

Fig. 11 Convergence of numerical solution; maximum laser intensity, $I_0 = 1.5 \times 10^{10}$ W/m^2. CFL = 4.0.

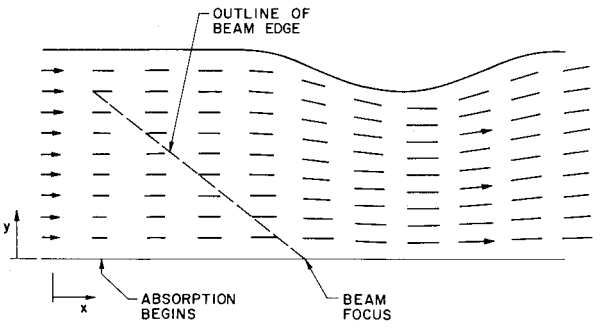

Fig. 12 Velocity vector plot for a laser intensity of $I_0 = 1.5 \times 10^{10}$ W/m^2. For clarity, velocities are shown at only every other grid point. (Flow is from left to right.)

which consistently shows the largest change is the one corresponding to the x-momentum equation. These results clearly indicate the solution procedure is converging. Additional convergence could, of course, be obtained by continuing the time-marching procedure. Representative calculations verified that the change $\Delta Q/Q$ could be driven to machine accuracy ($\Delta Q/Q \simeq 1 \times 10^{-15}$) if the computations were continued far enough. This additional convergence caused no notable difference in the plotted results.

A final point of interest is the effect of the laser absorption region on the fluid flow streamlines. The printed outputs clearly show that the effect of the laser absorption is to deflect the flow away from the centerline toward the walls. This effect, however, remains quite weak, and the flow angles in the vicinity of the heat addition zone are never more than 20% of the peak values observed at the wall because of the nozzle convergence (i.e., they are one-fifth the maximum wall slope). Peak flow angles of about 6 deg were observed in the heat addition region for the $I_0 = 1.5 \times 10^{10}$ W/m^2 case. An attempt at showing this graphically is presented in Fig. 12. Here velocity vectors for the magnitude and direction of the flow are given at every other grid point in the field. A hint of the downward velocity components can be seen in the heat addition zone, but the flow angles remain too small to be distinctive on this type of plot.

Summary

This paper has presented for the first time complete two-dimensional solutions for the laser/gasdynamic interaction in a beamed energy propulsion device. The calculations have included the effects of beam focusing, cross-beam intensity profiles, and real gas properties including transport effects. The analysis has been simplified by considering only constant gas absorptivity.

A dual grid system has been used for the numerical solutions. The fluid dynamic equations are solved in a body-fitted coordinate system which transforms the nozzle contour into a rectangular computational domain in which equal grid spacing can be used. The radiation conservation equations are solved in a coordinate system which follows each ray. The fluid dynamic equations are solved by an implicit, time-marching procedure with viscous terms treated explicitly. Boundary conditions are enforced by a procedure based upon the unsteady method of characteristics. Slip boundary conditions have been used at the nozzle walls to avoid having to resolve the boundary layers. This allows concentration to be focused on the absorption region.

Converged solutions have shown the expected high-temperature zone in the center of the nozzle with cool flow near the walls. The corresponding temperature profiles have steep gradients in both the streamwise and cross-stream directions and clearly show the need for the two-dimensional treatment. The presence of the absorption region acts as a blockage to the nozzle flow. As increased quantities of energy are absorbed in the gas, the mass flow through the

unchoked nozzle decreases, and the inlet velocity profile becomes strongly nonuniform with a low-velocity region near the nozzle centerline upstream of the absorption region. The streamlines are also deflected away from the centerline as they approach the absorption region.

Several specific simplifications should be noted. First, the calculations are for an unchoked nozzle. Extension to choked conditions is straightforward, and it is reasonable to expect that convergence can be obtained in the presence of similar laser powers. The second simplification is in the use of a constant absorptivity. The primary physical drawback to this simplification is that it removes the physical propagation mechanisms from the computations. Thus, it is impossible to predict effects such as the speed of propagation of an absorption region and the manner in which it varies with flow and laser conditions. Steps to extend the present analysis to include this important parameter are currently in progress, however, the present calculations are viewed as necessary first steps. The third simplification is the omission of the boundary-layer effects at the walls. This has an indirect effect on the mixing between the hot and cold gas, but studies of the mixing must be delayed until the absorption process is better understood. Finally, the effect of radiant emission from the hot sections (and its possible reabsorption by the surrounding cooler gases) has also been omitted. Although inclusion of emission would require more computations per time-step, its inclusion should have no adverse effect on the convergence of the calculation.

Acknowledgments

This work was partially sponsored by the Air Force Office of Scientific Research under Grant Number AFOSR 82-0196 and by NASA through Computational Fluid Dynamics Training Grant NGT 39-009-802.

References

[1]Jones, L. W. and Keefer, D. R., "NASA's Laser Propulsion Project," *Astronautics & Aeronautics*, Vol. 20, Sept. 1983, pp. 66-73.

[2]Kemp, N. H. and Krech, R. H., "Laser-Heated Thruster-Final Report," NASA CR-161666, Physical Sciences, Inc., Woburn, Mass., Sept. 1980.

[3]Kemp, N. H., "Simplified Models of CW Laser-Heated Thrusters," AIAA Paper 81-1249, Palo Alto, Calif., June 1981.

[4]Merkle, C. L., "The Potential for Using Laser Radiation to Supply Energy for Propulsion," *Progress in Astronautics and Aeronautics—Orbit Raising and Maneuvering Propulsion: Research Status and Needs*, Vol. 89, edited by L. H. Caveny, AIAA, New York, 1984, pp. 48-72.

[5]Raizer, Yu. P., *Laser-Induced Discharge Phenomena*, edited by G. C. Vlases and Z. A. Pietrzyk, Consultants Bureau, New York, 1977, pp. 26-44.

[6]Boni, A. A. and Su, F. Y., "Propagation of Laser-Supported Deflagration Waves," *Physics of Fluids*, Vol. 17, Feb. 1974, pp. 340-342.

[7]Jackson, J. P. and Nielsen, P. E., "Role of Radiation Transport in the Propagation of Laser-Supported Combustion Waves," *AIAA Journal*, Vol. 22, Nov. 1974, pp. 1498-1501.

[8]Kemp, N. H. and Root, R. G., "Analytical Study of Laser-Supported Combustion Waves in Hydrogen," *Journal of Energy*, Vol. 3, Jan.-Feb. 1979, pp. 40-49.

[9]Kemp, N. H. and Lewis, P. F., "Laser-Heated Thruster-Interim Report," NASA CR-161665, Physical Sciences, Inc., Woburn, Mass., Feb. 1980.

[10]Gulati, A. and Merkle, C. L., "The Absorption of Electromagnetic Radiation in an Advanced Propulsion System," *Journal of Spacecraft and Rockets*, Vol. 21, Jan.-Feb. 1984, pp. 101-107.

[11]Keefer, D., Peters, C., and Crowder, H., "A Reexamination of the Laser-Supported Combustion Wave," AIAA Paper 83-1444, June 1983.

[12]Keefer, D. R., Crowder, H., and Elkins, R., "A Two-Dimensional Model of the Hydrogen Plasma for a Laser-Powered Rocket," AIAA Paper 82-0404, Jan. 1982.

[13]Merkle, C. L., "Prediction of the Flowfield in Laser Propulsion Devices," *AIAA Journal*, Vol. 22, Aug. 1984, pp. 1101-1107.

[14]McCay, T. D. and Thoenes, J., "Numerical Modeling of Laser Thermal Propulsion Flows," *Progress in Astronautics and Aeronautics—Orbit Raising and Maneuvering Propulsion: Research Status and Needs*, Vol. 89, edited by L. H. Caveny, AIAA, New York, 1984, pp. 149-166.

[15]Degani, D., "Numerical Study of the Effect of an Embedded Surface-Heat Source on the Separation Bubble of Supersonic Flow," AIAA Paper 83-1753, July 1983.

[16]Beam, R. M. and Warming, R. F., "An Implicit Factored Scheme for the Compressible Navier-Stokes Equations," *AIAA Journal*, Vol. 16, April 1978, pp. 393-402.

[17]Briley, W. R. and McDonald, H., "Solution of the Multidimensional Compressible Navier-Stokes Equations by a Generalized Implicit Method," *Journal of Computational Physics*, Vol. 24, 1977, pp. 372-397.

[18]Douglas, J. and Gunn, J. E., "A General Formulation of Alternating Direction Methods, Part I, Parabolic and Hyperbolic Problems," *Numerische Mathematik*, Vol. 6, 1964, pp. 428-453.

[19]Chakravarthy, S. R., "Euler Equation-Implicit Schemes and Implicit Boundary Conditions," AIAA Paper 82-0228, Jan. 1982.

[20]Rai, M. M. and Chaussee, D. S., "New Implicit Boundary Procedures: Theory and Applications," *AIAA Journal*, Vol. 22, Aug. 1984, pp. 1094-1100.

[21]Keefer, D., Elkins, R., Peters, C., and Jones, L., "Laser Thermal Propulsion," *Progress in Astronautics and Aeronautics—Orbit Raising and Maneuvering Propulsion: Research Status and Needs*, Vol. 89, edited by L. H. Caveny, AIAA, New York, 1984, pp. 129-148.